Band structure calculations for dilute nitride quantum wells under compressive or tensile strain

2004 J. Phys.: Condens. Matter 16 S3215

(http://iopscience.iop.org/0953-8984/16/31/016)

INSTITUTE OF PHYSICS PUBLISHING JOURNAL OF PHYSICS: CONDENSED MATTER

J. Phys.: Condens. Matter **16** (2004) S3215–S3227 PII: S0953-8984(04)75828-2

Band structure calculations for dilute nitride quantum wells under compressive or tensile strain

H Carrère[1], X Marie[1], J Barrau[1], T Amand[1], S Ben Bouzid[2], V Sallet[2] and J-C Harmand[2]

[1] LNMO–INSA, 135 avenue de Rangueil, 31077 Toulouse cedex 4, France
[2] LPN, Route de Nozay, 91460 Marcoussis, France

Received 5 February 2004
Published 23 July 2004
Online at stacks.iop.org/JPhysCM/16/S3215
doi:10.1088/0953-8984/16/31/016

Abstract

We have calculated the band structure of InGaAsN/GaAs(N)/GaAs compressively strained quantum wells (QW) emitting at 1.3 μm using the band anticrossing model and an eight-band $\mathbf{k}\cdot\mathbf{p}$ Hamiltonian. The calculated interband optical transition energies have been compared to the experimental ones deduced from photocurrent, photoluminescence and excitation of photoluminescence spectroscopy experiments and measured laser characteristics extracted from the recent literature. Because of the high compressive strain in the QW, strain-compensated structures may be required in order to grow stable multiple QWs; in view of this we have studied the band structure of InGaAsN/GaAsP/GaAs QWs emitting at 1.3 μm. Dilute nitride structures also offer the possibility of growing tensile strained QW lasers on InP substrate emitting in the 1.55 μm emission wavelength range. In order to evaluate the potentialities of such structures we have determined the band characteristics of InGaAsN/InGaAsP/InP heterostructures with a TM polarized fundamental transition.

1. Introduction

Dilute quaternary group-III arsenide nitride compounds $In_xGa_{1-x}As_{1-y}N_y$ have been intensively studied in the past few years because of both their fundamental properties [1, 2] and their potential for 1.3 μm laser applications [3, 4].

Many laser devices have now been fabricated but their performances are often limited by the presence of nitrogen, responsible for non-radiative recombination centres and linewidth enlargement [3, 5–10]. Thus, the best quality QWs are usually obtained for high indium contents ($x > 0.3$) and low nitrogen contents ($y < 0.01$). These characteristics, combined with the growth of multiple-quantum-well (MQW) structures, yield a stronger intensity emission at 1.3 μm for room temperature operation. However, the number of QWs in such structures

may be limited because of the high compressive strain ($\Delta a/a \approx 2\%$) in the quaternary layer. Hence, growth would be facilitated and the number of QWs increased using strain-compensated heterostructures, with barriers under tensile strain, such as GaAsP ($\Delta a/a \approx -0.9\%$ for $GaAs_{0.8}P_{0.2}$ /GaAs).

The InGaAsN alloy, grown under tensile strain on InP substrate, also provides the possibility of reaching TM mode emission at 1.55 μm and above in the telecommunication L band which is difficult to reach with standard InGaAsP strained QW structures. Then the InGaAsN/InP system combined with confinement layers such as InAsP could lead to the fabrication of tensile strained QW lasers as well as the development of optical isolators requiring TM polarization [11, 12].

The design of InGaAsN based devices requires a deep knowledge of the alloy electronic properties and development of accurate models. The dramatic band gap reduction induced by the incorporation of nitrogen in the host matrix has been intensively investigated since it was first published [5] and many experimental and theoretical studies have led to a good understanding of the material properties. High hydrostatic pressure experiments performed by Shan *et al* [1, 13] have shown that incorporation of small amounts of nitrogen into conventional III–V compounds leads to a splitting of the conduction band into two subbands and an almost unchanged valence band structure. The observed effects were very nicely explained by the band anticrossing (BAC) model taking into account the strong coupling between the extended conduction band states close to the zone centre and the localized nitrogen states. Many electronic properties of InGaAsN structures such as the enlarged electron effective mass are well predicted using this simple two-level BAC approach [14]. More sophisticated calculations based on the pseudopotential supercell technique have recently confirmed the localized–delocalized duality of the conduction band edge in III–V nitride alloys [2, 15].

In this paper, we calculate the characteristics of InGaAsN QW structures on the basis of the BAC model and the $\mathbf{k} \cdot \mathbf{p}$ approximation. In section 2, we investigate the band structure of strained InGaAsN/GaAs QW structures. Calculated data are compared to photocurrent spectroscopy measurements performed on a high quality InGaAsN/GaAs QW and to further validate our parameters we compare our calculations of the fundamental e_1–hh_1 transition to more than 30 QWs extracted from the recent literature.

In section 3 we focus on the band structure of strained InGaAsN/GaAsN and strain-compensated InGaAsN/GaAsP QW heterostructures in order to evaluate their performances for 1.3 μm laser emission and compare them to the ones of InGaAsN/GaAs structures.

Finally, section 4 is dedicated to a preliminary study of the fundamental transition of TM polarized 1.55 μm emitting InGaAsN/InP and InGaAsN/InAsP QWs under tensile strain. All the calculations presented in this paper are performed for $T = 300$ K.

2. InGaAsN/GaAs quantum wells

First, we have calculated the band structure of $In_xGa_{1-x}As_{1-y}N_y$/GaAs QWs by solving the Lüttinger–Kohn Hamiltonian, including tetragonal strain and strong coupling between the InGaAs conduction band (CB) and the localized nitrogen levels. The eigenvalue problem is solved by the transfer-matrix method, taking into account the interfacial discontinuity condition [16, 17]. The valence band (VB) material parameters used for the calculations are those of InGaAs [18]. As far as the conduction band in concerned, calculations were started with the parameters determined by Shan *et al* [13]:

$$E_N = 1.65 - x(0.5 - 0.4x) \text{ eV} \quad (1)$$

for the nitrogen level energy (relative to the top of the valence band of unstrained InGaAs) and

$$V_{\mathrm{NM}} = 2.7\sqrt{y}\ \mathrm{eV} \tag{2}$$

for the coupling parameter in the BAC approach. As pointed out in [19], a systematic error was found between experiments and calculations. It is emphasized that the E_{N} and V_{NM} values mentioned above have been accurately determined for InGaAsN thick layers with low In content (<0.08) [13]. Indeed, for InGaAsN/GaAs QWs designed for 1.3 μm emission, the In fraction is much larger (about 0.3) and the validity of these parameters is questionable [19, 20]. We have obtained a reasonable agreement between the experiments and calculations either by including

(i) an additional In dependence of the nitrogen level position (E_{N} decreases when the In fraction increases)—note that Choulis *et al*, in their $\mathbf{k}\cdot\mathbf{p}$ calculations, took the energy separation between the nitrogen level and the bottom of the conduction band to be independent of the In composition in unstrained InGaAsN [20]; or
(ii) an In dependence of the V_{NM} coupling parameter (V_{NM} increases when the In fraction increases).

Hypothesis (ii) has already been suggested by Potter *et al* [21]. A coupling parameter of $V_{\mathrm{NM}} = 3.2\sqrt{y}$ eV has been determined by these authors for an In fraction in the well of $x = 0.2$. A simple interpolation between $V_{\mathrm{NM}} = 2.7\sqrt{y}$ eV ($x = 0.08$) and $V_{\mathrm{NM}} = 3.2\sqrt{y}$ eV ($x = 0.2$) has thus been used in our calculations for the phenomenological In dependence of the coupling parameter; the energy of the nitrogen level is assumed to be constant relative to the vacuum level whatever the InGaAsN composition is [13]. The In fraction (x) dependence of E_{N} in equation (1) just reflects the variation of the valence band offset with respect to GaAs [18].

It is clear that the BAC model used here with the above-mentioned V_{NM} and E_{N} parameters corresponds to an oversimplified description of the microscopic properties of InGaAsN material. As pointed out recently, the N-atom nearest-neighbour configuration in the alloy plays a crucial role in the electronic properties: N atoms can be for instance bounded to four Ga atoms or to one In and three Ga atoms [2, 22]. The induced disorder results in significant changes in the coupling between the nitrogen levels and the conduction band [23, 24]. The V_{NM} and E_{N} parameters used in the present paper or in [4, 20, 25] thus correspond to average values over the different configurations.

In order to validate our parameters, we have compared the calculated value of the e_1–hh_1 transition energy (using the V_{NM} and E_{N} parameters mentioned above) to experimental data extracted from the recent literature [3, 10, 14, 26–42]. The QW characteristics studied are reported in table 1, affording a large panel of well width (L_{W}), In content (x) and N content (y). According to the different authors, the experimental e_1–hh_1 transition wavelengths (λ_{exp}) were determined from photocurrent (PC), photoluminescence (PL) or excitation of photoluminescence (PLE) spectroscopy experiments and measured laser characteristics. The last column, indicating the error percentage ($(\lambda_{\mathrm{calc}} - \lambda_{\mathrm{exp}})/\lambda_{\mathrm{exp}}$) between the calculated and measured wavelengths, is plotted in a histogram in figure 1. According to the Gaussian fit, it appears that most of the experimental results are reasonably predicted by the calculation, within an error percentage of $\pm 2\%$. We emphasize that the calculations have been performed with the nominal parameters (L_{W}, x, y) given by the authors. Possible sources of error are:

(i) from the experimental side, the problematic experimental estimation of the N content of the QWs and the slight wavelength emission blue-shift induced by *in situ* annealing during the growth of cap layers;

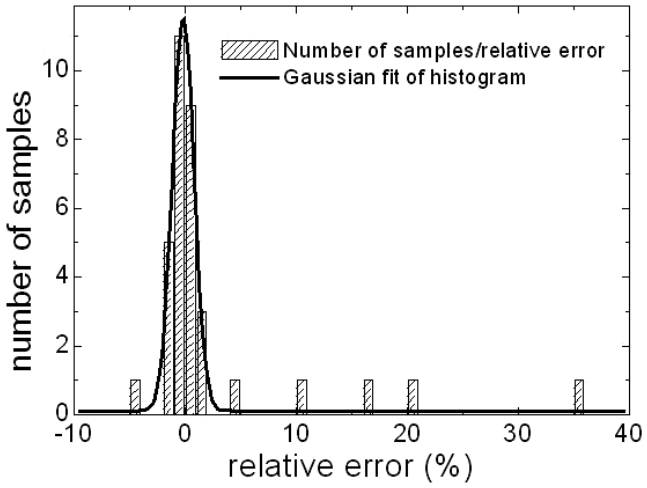

Figure 1. Comparison between the calculated e_1–hh_1 transition energy and experimental data extracted from the literature at room temperature (see table 1).

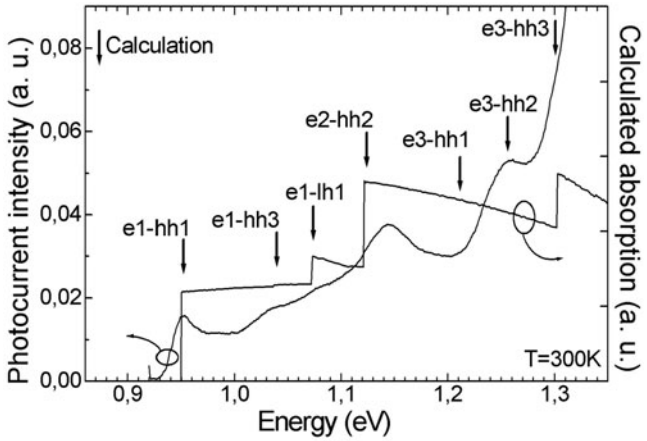

Figure 2. Comparison between calculated transition energies and PC measurements for a 7 nm $In_xGa_{1-x}As_{1-y}N_y$ /GaAs QW with $x = 0.37$, $y = 0.007$ at room temperature.

(ii) from the calculation side, the oversimplified BAC approach which does not take into account the different N-atom nearest-neighbour configurations.

In summary our calculations give satisfactory results in the limit of low N contents ($y < 0.015$) for the e_1–hh_1 transition energy value. Additional experimental work has then been done to validate the model for the higher e_i–$hh_j(lh_j)$ transition energies. We have grown a PIN structure containing a 7 nm $In_xGa_{1-x}As_{1-y}N_y$/GaAs QW with $x = 0.37$, $y = 0.007$ by plasma assisted molecular beam epitaxy (MBE). The growth temperature was kept constant at 600 °C for the whole structure and reduced to 450 °C for the QW. We have performed PC spectroscopy measurements using a tungsten lamp associated with a monochromator as the light source. The measured PC spectrum is reported in figure 2 (left y-axis) as well as the calculated e_i–$hh_j(lh_j)$ transition energies. The calculated absorption spectrum of the structure is also reported (right y-axis); note that this result has been obtained from the dipole matrix

Table 1. Literature references from which InGaAsN/GaAs e_1–hh_1 transition values were extracted, including PL, PC, PV and laser spectroscopy measurements at room temperature. The calculated transition and the error percentage are also displayed.

				e_1–hh_1		
References	x	y	L_W (nm)	λ_{exp} (μm)	λ_{calc} (μm)	Error (%)
[10]	0.3	0.005	6	1.156	1.163	0.6
	0.3	0.0082	6	1.231	1.235	0.3
	0.3	0.012	6	1.325	1.321	−0.3
[26]	0.34	0.007	7	1.261	1.276	1
[3]	0.1	0.02	7	1.226	1.164	−5
[27]	0.3	0.003	7	1.142	1.131	−0.96
[28]	0.3	0.003	7	1.155	1.131	−2
[29]	0.35	0.003	8	1.195	1.195	0
	0.37	0.003	8	1.231	1.217	−1
	0.37	0.005	8	1.265	1.275	0.8
[30]	0.39	0.005	6.6	1.28	1.278	−0.15
	0.37	0.005	7.7	1.294	1.271	−1.7
[31]	0.3	0.009	6.2	1.255	1.257	0.15
[32]	0.3	0.01	7	1.322	1.295	−2
[33]	0.32	0.004	6.5	1.163	1.168	0.4
	0.34	0.004	7.5	1.21	1.205	−0.4
	0.33	0.004	7.0	1.181	1.186	0.4
[34]	0.2	0.017	6.2	1.150	1.267	10
	0.3	0.028	6.2	1.270	1.72	35
[35]	0.31	0.01	8.0	1.3	1.324	1.8
[36]	0.32	0.01	10.0	1.319	1.344	1.8
[37]	0.36	0.015	6.0	1.27	1.544	20
[38]	0.3	0.02	7.0	1.33	1.553	16
[39]	0.33	0.01	10.0	1.32	1.379	4.4
[14]	0.3	0.005	4.0	1.107	1.113	0.5
	0.3	0.005	5.0	1.143	1.142	−0.08
	0.3	0.005	6.0	1.164	1.163	−0.08
	0.3	0.005	6.8	1.180	1.175	−0.4
	0.3	0.005	9.0	1.204	1.200	−0.3
[40]	0.36	0.0067	8.0	1.326	1.310	−1.2
	0.36	0.0078	8.0	1.355	1.341	−1
[41]	0.4	0.005	6	1.274	1.278	−0.3
[42]	0.36	0.005	6.5	1.24	1.24	0
	0.36	0.008	6.5	1.298	1.320	−1.7

element calculations—neither the excitonic effect nor the inhomogeneous broadening were taken into account. We find a good agreement between the theoretical and experimental transition energies for the low energy range (e_1–hh_1 to e_2–hh_2); the identification of higher energy transitions is questionable.

3. InGaAsN/GaAsN and InGaAsN/GaAsP quantum wells

The incorporation of nitrogen in the GaAs barriers induces a decrease of the InGaAsN QW conduction band offset due to the large band gap reduction. This barrier height reduction should induce a slight decrease of the electron confinement energies. Then, the 1.3 μm emission wavelength should be reached for slightly lower N content in the QW. Note that

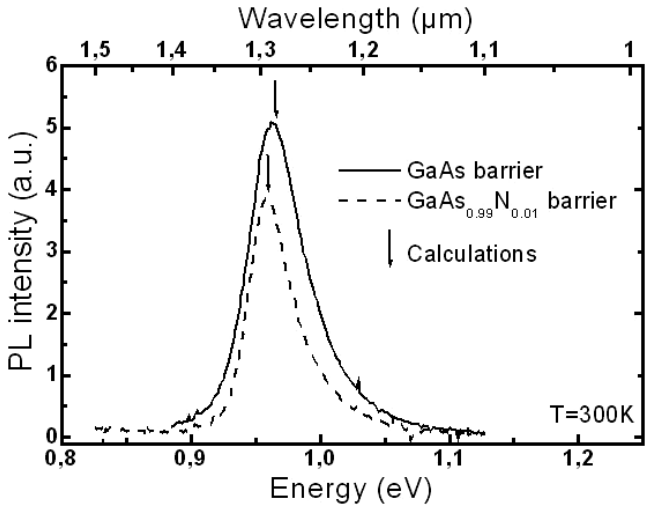

Figure 3. Comparison between calculated transition energies and PL measurements for 7 nm $In_{0.345}Ga_{0.655}As_{0.993}N_{0.007}$ QWs with GaAs (solid curve) and $GaAs_{0.99}N_{0.01}$ (dashed curve) barriers at room temperature.

Table 2. Literature references from which InGaAsN/GaAsP e_1–hh_1 transition values were extracted, including PL, PC, PV and laser spectroscopy measurements at room temperature.

					e_1–hh_1		
References	Barrier	x	y	L_W (nm)	λ_{exp} (μm)	λ_{calc} (μm)	Error (%)
[43]	$GaAs_{0.8}P_{0.2}$	0.4	0	7	1.15	1.14	−0.9
		0.4	0.005	7	1.185	1.22	2.9
		0.4	0.007	7	1.20	1.27	5.5
		0.4	0.009	7	1.24	1.33	6.8
[41]	GaAs	0.4	0.005	6	1.274	1.278	0.3
	$GaAs_{0.85}P_{0.15}$	0.4	0.005	6	1.26	1.27	0.8

the GaAsN barriers are under tensile strain but the lattice mismatch ($\Delta a/a \approx -0.2\%$ for a N fraction of $\sim$0.01) is not sufficient for growing strain-compensated structures. In contrast, adding P to the GaAs barriers induces a large increase of the band offset and the lattice mismatch ($\Delta a/a \approx -0.9\%$ for $GaAs_{0.8}P_{0.2}$/GaAs) should allow the growth of stable strain-compensated InGaAsN MQW structures.

We have extended the model presented in section 2 to InGaAsN/GaAsN and InGaAsN/GaAsP heterostructures. The calculation follows the same approach as the one developed previously for InGaAsN/GaAs; the only changed data are the barrier characteristics. We have compared our calculated data to the few available in the literature (table 2) [41, 43]. A rather good agreement is found for low N content InGaAsN/GaAsP QWs.

In order to validate the InGaAsN/GaAsN calculations, we have grown two 7 nm thick InGaAsN QW samples by MBE, one with GaAs barriers and the other one with $GaAs_{0.99}N_{0.01}$ barriers. The QW characteristics are the same for the two samples. From the growth conditions and structural characterizations the In and N fractions in the QWs were estimated to be in the ranges $0.3 < x < 0.35$ and $0.005 < y < 0.007$, respectively. The PL emission spectra of these two samples are reported in figure 3. First, we have run the calculation to find the best

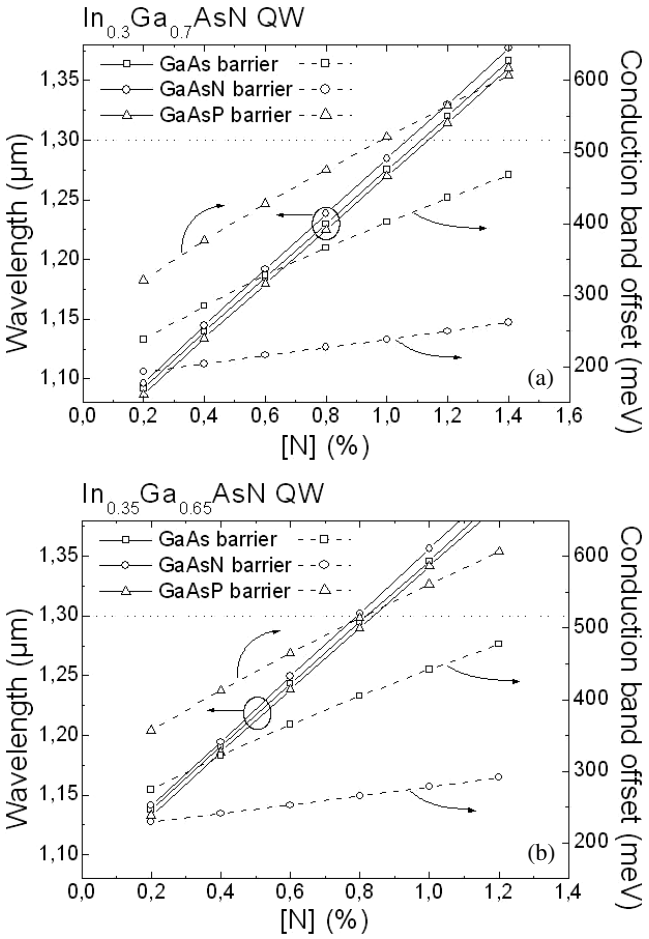

Figure 4. The calculated wavelength emission (solid lines) and conduction band offset (dashed lines) for 6 nm $In_xGa_{1-x}As_{1-y}N_y/GaAs$ (squares), $In_xGa_{1-x}As_{1-y}N_y/GaAs_{1-y}N_y$ (circles) and $In_xGa_{1-x}As_{1-y}N_y/GaAs_{0.8}P_{0.2}$ (triangles) QWs as a function of y for (a) $x = 0.3$ and (b) $x = 0.35$ at room temperature.

In–N content combination in the QW for the N-free barrier sample; the best fit was found for $x = 0.345$ and $y = 0.007$ (these values are in the intervals deduced from the growth conditions). We then injected these data into the calculation of the InGaAsN/GaAsN QW, the computed QW contents being $x = 0.345$ and $y = 0.007$ and the N content in the barrier being $y = 0.01$. The calculated values of the PL peaks are reported in figure 3 (vertical arrows). The calculation predicts a 5 meV red-shift of the fundamental transition on adding 1% of N in the barrier and the experiment shows a 4 meV red-shift of the PL peak emission. Note that the same kind of red-shift was calculated by Hader *et al* [44] in InGaAsN/InGaAsN QWs.

From the successful comparison of our calculations to a large panel of experimental data, it appears that we can use this model as an accurate tool for design of dilute nitride QW devices. We then calculated the e_1–hh_1 transition energy and the conduction band offset for 6 nm $In_xGa_{1-x}As_{1-y}N_y$ QWs with $x = 0.3$ (figure 4(a)) and $x = 0.35$ (figure 4(b)), varying y in order to reach 1.3 μm emission wavelength. These parameters have been chosen with a view to minimizing the N content and limiting the compressive strain in the QW. For the

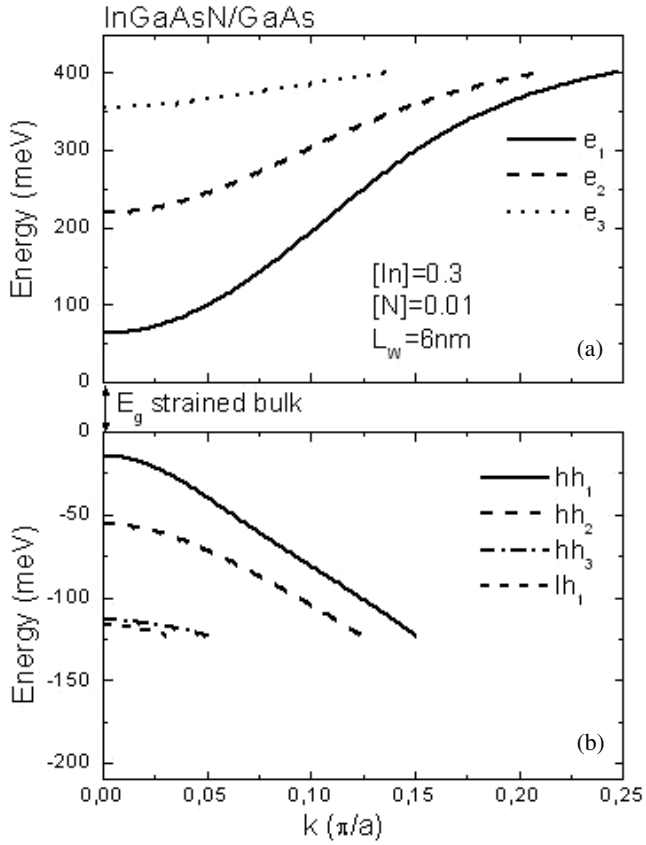

Figure 5. Conduction and valence band dispersion curves in the layer plane for 6 nm $In_{0.3}Ga_{0.7}As_{0.99}N_{0.01}$/GaAs QW structure at room temperature.

InGaAsN/GaAsN QW the N content in the barrier was fixed to the same value as for the QW in order to take into account growth constraints. For the InGaAsN/GaAsP QW the P content was chosen to be 0.2 which corresponds to the value used for recent MBE growth of such samples [43].

From figure 4(a) it can be seen that for a 6 nm thick $In_{0.3}Ga_{0.7}As_{1-y}N_y$ QW under compressive strain ($\Delta a/a \approx 1.9\%$) the N content has to be set to about 0.01 to reach 1.3 μm emission wavelength. The barrier height, fixed by the N or P content, has a rather low influence upon the e_1–hh_1 transition energy. In contrast, it appears clearly that the incorporation of P in the barrier induces as expected a large increase of the conduction band offset whereas the presence of N in the barrier induces a dramatic drop of this latter. The same trends can be observed for an $In_{0.35}Ga_{0.65}As_{1-y}N_y$ QW (figure 4(b)). Increasing the In fraction allows 1.3 μm emission for lower N contents, which may induce a better material quality. This configuration can be used for single-QW based applications; however, the compressive strain is also increased ($\Delta a/a \approx 2.25\%$) which may raise stability problems. Hence, the $In_{0.3}Ga_{0.7}As_{1-y}N_y$/GaAsP system appears to be a good candidate for laser application, offering a large electron band offset (and hence good T_0 characteristics) as well as strain compensation for MQW structures.

Figures 5 and 6 display as examples the valence band and conduction band dispersion curves in the layer plane for an $In_{0.3}Ga_{0.7}As_{0.99}N_{0.01}$/GaAs (figure 5) and an

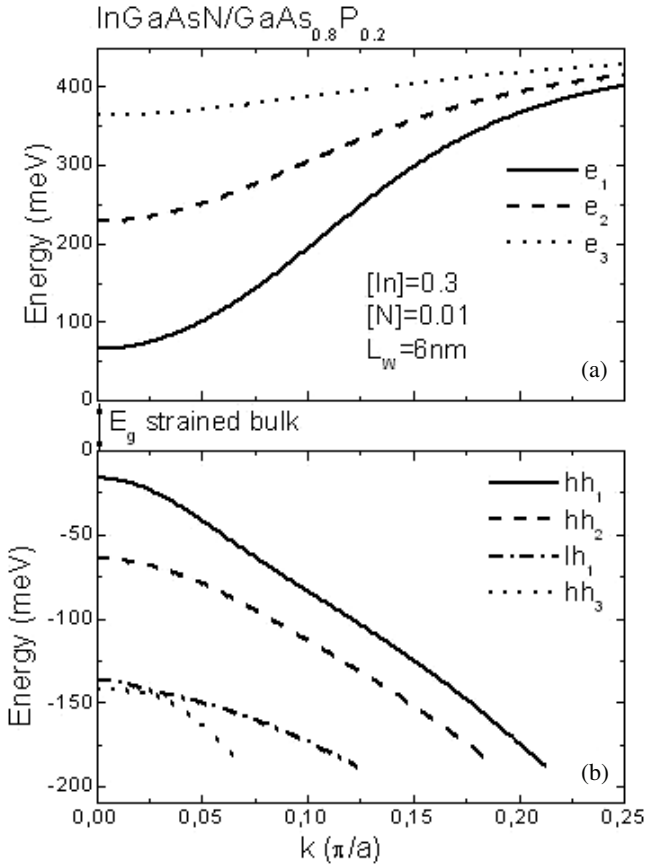

Figure 6. Conduction and valence band dispersion curves in the layer plane for 6 nm $In_{0.3}Ga_{0.7}As_{0.99}N_{0.01}/GaAs_{0.8}P_{0.2}$ QW structure.

$In_{0.3}Ga_{0.7}As_{0.99}N_{0.01}/GaAs_{0.8}P_{0.2}$ (figure 6) QW with a well width of $L_W = 6$ nm. The calculation of the hole states in the valence band in the case of GaAsP barrier is stopped when the QW hole energies coincide with the continuum light hole states of the barrier. We note in figures 5 and 6 that, excepting the larger band offset in the case of GaAsP barriers, the dispersion curves for the first electron and hole subbands are very similar. The strong conduction band non-parabolicity and the increase of the electron mass in the zone centre due to the nitrogen incorporation are clearly observed (we find here $m_e \sim 0.075\ m_0$ close to the zone centre for the e_1 subband). The dispersion curve determination is a first step towards the calculation of the material gain for future laser applications.

4. InGaAsN/InP and InGaAsN/InAsP quantum wells

We finally calculated the band structure of InGaAsN QWs grown on InP substrates. It is well known that $In_xGa_{1-x}As$ can be grown lattice matched to InP for $x = 0.535$. Lowering In content or adding N into the alloy (in substitution for As) induces a tensile strain. A sufficiently high tensile strain will lead to a e_1–lh_1 fundamental transition, giving rise to TM mode polarization emission. The potential advantages of tensile strained quantum well lasers (in terms of threshold current density and loss mechanisms) were predicted more than

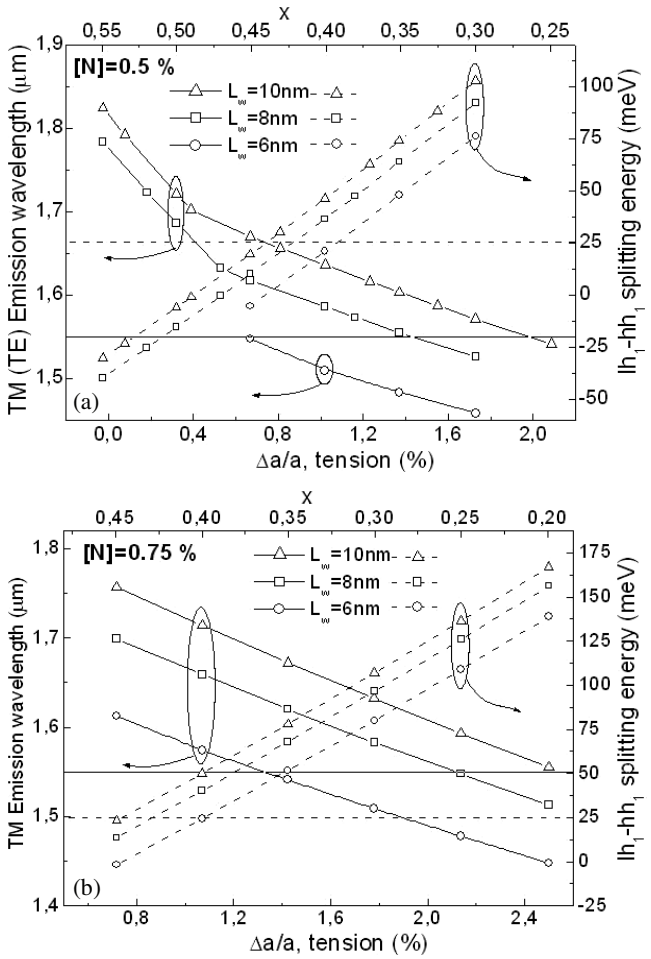

Figure 7. The calculated wavelength emission (solid line) and lh_1–hh_1 splitting energy (dashed line) for 6 nm (circles), 8 nm (squares) and 10 nm (triangles) $In_xGa_{1-x}As_{1-y}N_y$/InP QWs as a function of x for (a) $y = 0.005$ and (b) $y = 0.0075$. The solid (dashed) horizontal line corresponds to an emission wavelength of 1.55 μm (splitting energy lh_1–$hh_1 = 25$ meV).

ten years ago [45–47]. It is thus interesting to evaluate the characteristics of InGaAsN quantum wells under tensile strain grown on InP substrate for 1.5–1.6 μm emission wavelength. Moreover, this structure can also be very useful for the fabrication of 1.55 μm optical isolators requiring TM polarization [11, 12]. The TE–TM polarization transition can be observed in figures 7(a) and (b). We have calculated the emission wavelength for $In_xGa_{1-x}As_{1-y}N_y$ /InP QWs (figure 7(a): $y = 0.005$; figure 7(b): $y = 0.0075$) as a function of the tensile strain (bottom x-axis); the corresponding In content is also reported (top x-axis). The N content was arbitrarily fixed at values lower than 0.01 in order to keep optimal material quality. In the low strain region of figure 7(a) (high In content), in spite of a deeper QW for the light holes than for the heavy holes, the fundamental transition energy is still e_1–hh_1, i.e. TE mode polarization emission, mainly due to the difference between the light and heavy hole effective masses along the growth axis. When increasing tensile strain, lh_1 becomes the first hole energy level; the slope change in the $x \sim 0.5$ region marks the change from an e_1–hh_1 to an e_1–lh_1

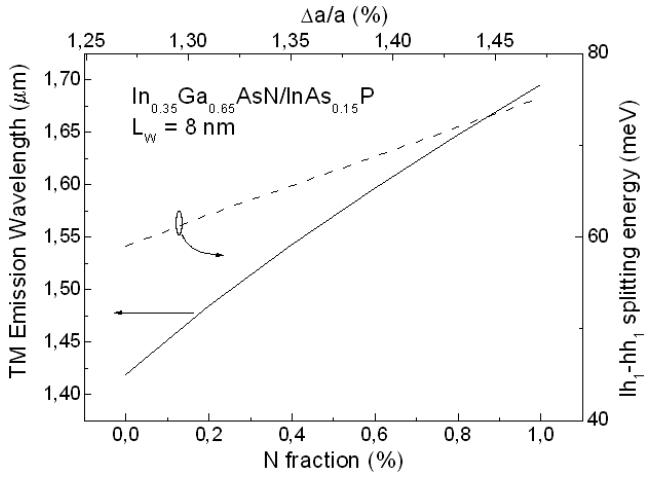

Figure 8. The calculated wavelength emission (solid line) and lh_1–hh_1 splitting energy (dashed line) for a 8 nm $In_{0.35}Ga_{0.65}As_{1-y}N_y/InAs_{0.15}P_{0.85}$ QW as a function of y.

transition. An additional condition for TM laser operation is a sufficient lh_1–hh_1 splitting energy: lh_1–$hh_1 > kT \sim 25$ meV at 300 K. For $y = 0.005$ (figure 7(a)) these conditions are obtained for $L_W \approx 7$ nm and above and $x < 0.4$. For $y = 0.0075$ (figure 7(b)) these conditions can be obtained for thinner QWs but lower In contents, inducing a higher strain ($\Delta a/a \approx 2.5\%$ for $In_{0.2}Ga_{0.8}As_{1-y}N_y$/InP). The lh_1–hh_1 splitting energy can also be increased by increasing L_W; however, a compromise has to be found between the lh_1–hh_1 splitting energy and the QW width as L_W has to be smaller than the critical thickness.

For growing MQW structures, compressively strained barriers such as InAsP may be suitable in order to

(i) form the optical confinement of the laser and
(ii) balance the tensile strain in the QW.

We have investigated 8 nm thick $In_{0.35}Ga_{0.65}As_{0.995}N_{0.005}/InAs_zP_{1-z}$ QWs with $z = 0.31$ and 0.15 grown on InP substrate. In the first case, the emission wavelength is 1.59 μm, the tensile strain in the QW ($\Delta a/a = 1.37\%$) may be well balanced by the compressive strain in the barrier ($\Delta a/a = 1\%$), the lh_1–hh_1 splitting energy is as high as 70 meV, but the CB offset drops down to 90 meV due to the high content of As in the barrier. Hence, this latter has to be reduced and $z = 0.15$ seems to be a good compromise. Indeed, in this case the emission wavelength is 1.57 μm, the tensile strain in the QW can still be balanced by the compressive strain in the barrier ($\Delta a/a = 0.48\%$), the lh_1–hh_1 splitting is 67 meV and the CB offset is increased to 167 meV. As an example relating to telecommunication L-band applications, we have plotted in figure 8 the TM emission wavelength and the lh_1–hh_1 splitting of a 8 nm $In_{0.35}Ga_{0.65}As_{1-y}N_y/InAs_{0.15}P_{0.85}$ QW as a function of y. The tensile strain in the QW is also reported as the top x-axis. It appears that TM mode emission at 1.55 μm and above can be reached with N fractions between 0.005 and 0.01, inducing a lattice mismatch smaller than 1.5%, a lh_1–hh_1 splitting higher than 60 meV and a CB offset higher than 160 meV. In these conditions, strain-compensated MQW laser structures may be successfully grown.

Very few experimental data are available in the literature for this system. We have compared our wavelength calculations to ones for an $In_{0.535}Ga_{0.465}As_{0.994}N_{0.006}/In_{0.535}Ga_{0.465}As$ MQW ($L_W = 20$ nm) grown on an InP substrate [48]. The experimental value at 300 K,

extrapolated from the low temperature PL, is 1.932 μm when the calculated wavelength is 1.916 μm; i.e. there is a relative error of -0.8%. This encouraging result has of course to be further confirmed with future experimental data.

5. Conclusion

We have calculated the InGaAsN/GaAs band structure using the BAC model and the $\mathbf{k} \cdot \mathbf{p}$ approximation in the Lüttinger–Kohn approach, i.e. taking into account the effects of strain, quantum confinement and the strong coupling between the localized nitrogen states and the extended states of the InGaAs conduction band. Comparing our theoretical results to experimental data extracted from the recent literature, it appears that the present model predicts the e_1–hh_1 transition energy within a relative error of $\pm 2\%$. Comparison to PC spectroscopy measurement has also shown a very good agreement for higher transition energies. These calculations can thus be used as an accurate tool for designing laser devices. We have extended the model to InGaAsN QWs sandwiched between GaAsN or GaAsP barriers. It comes out that the InGaAsN/GaAsP system can, attractively, be used in 1.3 μm MQW lasers, as the high compressive strain in the InGaAsN layer is partly balanced by the tensile strain in the barrier material. The InGaAsN material grown under tensile strain on InP substrate is also a very good candidate for 1.55 μm applications. First, combined with InAsP barriers, it provides the possibility of reaching telecommunication L-band emission and, second, the TM mode emission can be used in optical isolator devices.

Acknowledgments

This work was supported by the French Ministry of Research: RNRT programme (AHTOS project). We are grateful to A Arnoult, N Balkan and R Potter for fruitful discussions.

References

[1] Shan W, Walukiewicz W, Ager J W III, Haller E E, Geisz J F, Friedman D J, Olson J M and Kurtz S R 1999 *Phys. Rev. Lett.* **82** 1221–4
[2] Kim K and Zunger A 2001 *Phys. Rev. Lett.* **86** 2609–12
[3] Kondow M, Uomi K, Niwa A, Kitatani T, Wakahiki S and Yazawa Y 1996 *Japan. J. Appl. Phys.* **35** 1273–5
[4] Hofmann M, Wagner A, Ellmers C, Schlichenmeier C, Schafer S, Hohnsdorf F, Koch J, Stolz W, Koch S W, Ruhle W, Hader J, Moloney J V, O'Reilly E P, Borchert B, Egorov A Y and Riechert H 2001 *Appl. Phys. Lett.* **78** 3009–11
[5] Weyers M, Sato M and Ando H 1992 *Japan. J. Appl. Phys.* 2 **31** L853–5
[6] Ougazzaden A, Le Bellego Y, Rao E V K, Juhel M, Leprince L and Patriarche G 1997 *Appl. Phys. Lett.* **70** 2861–3
[7] Kondow M, Uomi K, Niwa A, Kitatani T, Watahiki S, Yazawa Y, Hosomi K and Mozume T 1997 *Solid-State Electron.* **41** 209–12
[8] Xin H P and Tu C W 1998 *Appl. Phys. Lett.* **72** 2442–4
[9] Rao E V K, Ougazzaden A, Le Bellego Y and Juhel M 1998 *Appl. Phys. Lett.* **72** 1409–11
[10] Yang X, Heroux J B, Jurkovic M J and Wang W I 1999 *J. Vac. Sci. Technol.* B **17** 1144–6
[11] Takenaka M and Nakano Y 1999 *Proc. 11th Int. Conf. on Indium Phosphide and Related Materials* pp 289–92
[12] Zaets W and Ando K 1999 *IEEE Photon. Technol. Lett.* **11** 1012–4
[13] Shan W, Walukiewicz W, Yu K M, Ager J W III, Haller E E, Geisz J F, Friedman D J, Olson J M, Kurtz S R, Xin H P and Tu C W 2001 *Phys. Status Solidi* b **223** 75–85
[14] Pan Z, Li L H, Lin Y W, Dun Q, Jiang D S and Ge W K 2001 *Appl. Phys. Lett.* **78** 2217–9
[15] Kent P R C and Zunger A 2001 *Phys. Rev. Lett.* **86** 2613–6
[16] Epenga R, Schuurmans M F H and Colak S 1987 *Phys. Rev.* B **36** 1554–64
[17] Ahn D and Chuang S L 1990 *IEEE J. Quantum Electron.* **26** 13–23

[18] Marie X, Barrau J, Brousseau B, Amand T, Brousseau M, Rao E V K and Alexandre F 1991 *J. Appl. Phys.* **69** 812–5
[19] Marie X, Barrau J, Amand T, Carrère H, Arnoult A, Fontaine C and Bedel-Pereira E 2003 *IEE Proc., Optoelectron.* **150** 25–7
[20] Choulis S A, Hosea T J C, Tomic S, Kamal-Saadi M, Adams A R, O'Reilly E P, Weinstein B A and Klar P J 2002 *Phys. Rev.* B **66** 1653211–9
[21] Potter R J, Balkan N, Marie X, Carrère H, Bedel E and Lacoste G 2001 *Phys. Status Solidi* a **187** 623–32
[22] Klar P J, Grüning H, Koch J, Schäfer S, Volz K, Stolz W, Heimbrodt W, Kamal-Saadi M, Lindsay A and O'Reilly E P 2001 *Phys. Rev.* B **64** 121203(R)
[23] Alexandropoulos D and Adams M J 2003 *IEE Proc., Optoelectron.* **150** 40–4
[24] Alexandropoulos D and Adams M J 2003 *IEE Proc., Optoelectron.* **150** 105–9
[25] Hader J, Koch S W, Moloney J V and O'Reilly E P 2000 *Appl. Phys. Lett.* **77** 630–2
[26] Kageyama T, Miyamoto T, Makino S, Koyama F and Iga K 1999 *Japan. J. Appl. Phys.* 2 **30** L298–300
[27] Hains C P, Li N Y, Yang K, Huang X D and Cheng J L 1999 *IEEE Photon. Technol. Lett.* **11** 1208–10
[28] Yang K, Hains C P and Cheng J L 2000 *IEEE Photon. Technol. Lett.* **12** 7–9
[29] Kageyama T, Miyamoto T, Makino S, Nishiyama N, Koyama F and Iga K 2000 *IEEE Photon. Technol. Lett.* **12** 10–2
[30] Sato S and Satoh S 1999 *IEEE Photon. Technol. Lett.* **11** 1560–2
[31] Xin H P and Tu C W 1998 *Appl. Phys. Lett.* **72** 2442–4
[32] Kondow M, Kitatani T, Nakahara K and Tanaka T 1999 *Japan. J. Appl. Phys.* 2 **38** L1355–6
[33] Kageyama T, Miyamoto T, Makino S, Koyama F and Iga K 2000 *J. Cryst. Growth* **209** 350–4
[34] Egorov A Yu, Bernklau D, Borchert B, Illek S, Livshits D, Rucki A, Schuster M, Kaschner A, Hoffmann A, Dumitras Gh, Amann M C and Riechert H 2001 *J. Cryst. Growth* **227/228** 545–52
[35] Reinhardt M, Fischer M and Forchel A 2000 *Physica* E **7** 919–23
[36] Shirakata S, Kondow M and Kitatani T 2002 *Appl. Phys. Lett.* **80** 2087–9
[37] Markus A, Fiore A, Ganière J D, Oesterle U, Chen J X, Deveaud B, Ilegems M and Riechert H 2002 *Appl. Phys. Lett.* **80** 911–3
[38] Spruytte S G, Larson M C, Wampler W, Coldren C W, Petersen H E and Harris J S 2001 *J. Cryst. Growth* **227/228** 506–15
[39] Kitatani T, Kondow M and Tanaka T 2001 *J. Cryst. Growth* **227/228** 521–6
[40] Li L H, Patriarche G, Lemaitre A, Largeau L, Travers L and Harmand J C 2003 *J. Cryst. Growth* **251** 403–7
[41] Tansu N, Yeh J Y and Mawst L J 2003 *Appl. Phys. Lett.* **82** 3008–10
[42] Kudrawiec R, Sek G, Ryczko K, Misiewicz J, Sundgren P, Asplund C and Hammar M 2003 *Solid State Commun.* **127** 613–8
[43] Li W, Turpeinen J, Melanen P, Savolainen P, Uusimaa P and Pessa M 2001 *J. Cryst. Growth* **227/228** 541–4
[44] Hader J, Koch S W and Moloney J V 2003 *Solid-State Electron.* **47** 513–21
[45] Thijs P J A, Tiemeijer L F, Kuindersma K I, Binsma J J M and van Dongen T 1991 *IEEE J. Quantum Electron.* **27** 1426–39
[46] Thijs P J A, Tiemeijer L F, Binsma J J M and van Dongen T 1994 *IEEE J. Quantum Electron.* **30** 477–99
[47] O'Reilly E P, Jones G, Ghiti A and Adams A R 1991 *Electron. Lett.* **27** 1417–9
[48] Gokhale M R, Wei J, Wang H and Forrest S R 1999 *Appl. Phys. Lett.* **74** 1287–9